IOP Conf. Series: Materials Science and Engineering **269** (2017) 012070 doi:10.1088/1757-899X/269/1/012070

Microstructural and Microanalytical Study on Concrete Exposed to the Sulfate Environment

Fang Qing[1], Li Beixing[2*], Yin Jiangang[3], Yuan Xiaolu[4]

[1]Hubei Electric Power Survey & Design Institute, Wuhan, 430040, China
[2]State Key Laboratory of Silicate Materials for Architecture, Wuhan University of Technology, Wuhan, 430070, China
[3]State Grid Hubei Electric Power Company, Wuhan, 430077, China
[4]College of Civil Engineering and Architecture, China Three Gorges University, Yichang 443002, China

Abstract. Microstructural properties have been examined to investigate the effect of mineral admixtures on the sulfate resistance of concrete. Concrete and cement paste specimens made with ordinary Portland cement (OPC) or ordinary Portland cement incorporating 20% fly ash (FA) or 30% ground blast furnace slag (GBFS), were made and exposed to 250 cycles of the cyclic sulfate environment. Microstructural and Microanalytical study was conducted by means of x-ray diffraction (XRD), scanning electron microscope (SEM), energy dispersive spectroscopy (EDS) and mercury intrusion porosimetry (MIP). Results indicate that the pore structure of concrete after sulfate exposure possesses the fractal feature. The OPC concrete presents more complex pore internal surface, higher porosity and less micro-pores than the concrete incorporating fly ash and GBFS. Portlandite in OPC concrete and OPC-FA concrete is mainly converted to gypsum; while for OPC-GBFS concrete, both gypsum and ettringite are formed. In the cyclic sulfate environment, repeated hydration and dehydration of sulfates produce the expansive stress in pores, aggravating the demolishment of concrete structure.

1. Introduction

Deterioration of concrete structure exposed to sulfate-bearing environments such as seawater, soils or groundwater containing high concentration of sulfates, is known as sulfate attack, which is commonly observed. Sulfate attack is a quite complicated process. Sulfates diffuse into concrete and react with cement matrix including the calcium hydroxide and the calcium aluminate hydrate, forming the expansive products such as the ettringite and gypsum. This induces the expansion and cracking of concrete. It is also reported that the sulfate attack causes the decomposition of hydrated products such as the decalcification of C-S-H, leading to the disintegration of cement matrix [1-6].

Incorporation of mineral admixtures in concrete decreases the C3A quantity in cementitious materials, which reduces the potential for the formation of harmful products such as ettringite. The pozzolanic reaction of mineral admixtures partially consumes calcium hydroxide, and produces the secondary C-S-H gel to densify the microstructure of concrete [7-12]. Therefore, the presence of mineral admixtures is known to affect the sulfate resistance of concrete. The physical and mechanical properties of concrete incorporating mineral admixtures under the sulfate exposure have been studied in prior work [13, 14]. In this study, microstructure analyses are performed to investigate the effect of mineral admixtures on the deterioration mechanism of concrete subjected to sulfate attack.

2. Experimental

2.1. Materials

Ordinary Portland cement (OPC) was used. Class I fly ash (FA) with the specific surface area of 620m^2/kg and ground blast furnace slag (GBFS) with the specific surface area of 450m^2/kg were used as supplementary cementitious materials. Chemical compositions of cement, FA and GBFS are given in table 1. BASF SP-8CR superplasticizer with the water reducing rate of 25% was used at different dosages in mixes to achieve the adequate workability in concretes and pastes. River sand with the fineness modulus of 2.9 and the coarse aggregate of crushed limestone with the size of 5mm~25mm were used in making concrete. The analytically pure sodium sulfate was used to prepare the sulfate solution.

Table 1. Chemical analysis for cement, fly ash and ground blast furnace slag (wt. %)

Oxide/phase	SiO_2	Al_2O_3	Fe_2O_3	CaO	MgO	SO_3	Na_2O	K_2O	C_3S	C_2S	C_3A	C_4AF
OPC	21.78	4.85	3.36	65.66	2.61	0.58	0.19	0.56	58.71	17.22	7.17	10.21
FA	48.91	28.05	8.85	2.65	1.03	0.86	0.78	2.08	—	—	—	—
GBFS	32.69	15.50	1.70	38.14	9.14	1.73	0.10	0.43	—	—	—	—

Table 2. Concrete proportions.

Samples	Materials (kg/m^3)						
	Cement	Water	Sand	Stone	FA	GBFS	Superplasticizer
L-1	460	154	724	1086	0	0	4.6
L-2	384	154	724	1086	96	0	4.8
L-3	336	154	724	1086	0	144	4.8

2.2. Specimens preparation.

Mixture proportions used in making concretes and pastes are listed in tables 2 and 3, respectively. Three different binders were used in this study: 100%OPC, and 80%OPC-20%FA, 70%OPC-30%GBFS. A 0.335 water/binder (w/b) ratio was used for pure OPC concrete, and the w/b for concrete mixes with mineral admixtures was 0.32. Concretes (100×100×100 mm) and pastes (20×20×20 mm) were made and cured until 28d in accordance with the standard curing method described in GB/T 50081-2002 (Standard test method for mechanical properties km ordinary concrete). Before exposure to the sulfate environment, mercury intrusion porosimetry (MIP) of L-1 concrete and x-ray diffraction (XRD) of OPC paste were measured.

Table 3. Paste proportions.

Binders	w/b	Superplasticizer (%)
100%OPC	0.30	0.25
80% OPC-20% FA	0.29	0.25
70% OPC-30% GBFS	0.29	0.25

2.3. Experimental methods.

To accelerate the process of experiment, the cyclic sulfate exposure was applied for both concrete and paste specimens. One cycle was composed of drying at 80℃ for 6h, cooling at room temperature for 1h, exposure to the 10% Na_2SO_4 solution at (20±3)℃ for 16h and airing at room temperature for 1h. The container of the Na_2SO_4 solution was sealed. The solution was mixed everyday with constant regulation. The sulfate solution was refreshed every 7 cycles.

After 250 cycles of exposure, the paste samples were examined for the chemical components through x-ray diffraction (XRD). The spalling concrete was analyzed by scanning electron microscope (SEM), energy dispersive spectroscopy (EDS) and mercury intrusion porosimetry (MIP).

3 Results and discussion

3.1. MIP analysis

Pore structure, which relates to the physical and mechanical properties of concrete including the strength and the durability, includes some vital parameters such as the porosity and the pore size distribution. Table 4, figure 1 and figure 3 show the porosity and the pore size distribution of concrete specimens. It can be seen that the porosity of L-1 concrete subjected to 250 cycles of sulfate attack is decreased by more than 30%, compared with that before exposure. However, there are less micro-pores (<50 nm) in L-1 after exposure than that before exposure. This is possibly because that the expansive products such as gypsum and ettringite produced by the sulfate attack fill in pores of concrete, reducing the porosity of concrete. But these expansive products are not densely packed, contributing to big pores (100~200 nm and >200 nm) in concrete. The porosity of concrete is decreased with the addition of mineral admixtures. Compared with L-1 whose pores are mainly concentrated in big sizes (50~100 nm, 100~200 nm and >200 nm), L-2 and L-3 achieve the decreased pore distribution in >50 nm. Both of them have a largest pore distribution in <20 nm, which do little harm to the durability of concrete. This indicates that the incorporation of mineral admixtures improves the sulfate resistance of concrete, which possesses the lower porosity and more micro-pores after 250 cycles of sulfate attack than the OPC concrete. It is probably because that the pozzolanic reaction of GBFS and fly ash reduces the contents of $Ca(OH)_2$ and calcium aluminate hydrate in the cement paste and promotes the hydration of Portland cement, which together with the filler effect of mineral admixtures, make the matrix denser to safeguard against the external ingressive sulfates.

Table 4. Pore structure parameters of concrete.

Samples	Porosity (by volume) %	Pore distribution (by volume) %				
		<20 nm	20~50 nm	50~100 nm	100~200 nm	>200 nm
L-1(0)	13.64	36.35	29.34	15.85	5.02	13.44
L-1	9.04	29.91	17.12	9.12	6.96	36.88
L-2	7.72	46.19	12.53	3.54	3.15	34.57
L-3	7.08	44.28	14.32	4.71	4.07	32.61

L-1(0): L-1 before sulfate exposure; L-1: L-1 after sulfate exposure.

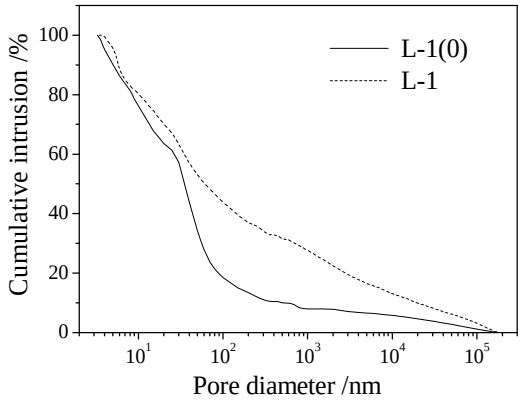

Figure 1. Pore size distribution of L-1 before and after exposure.

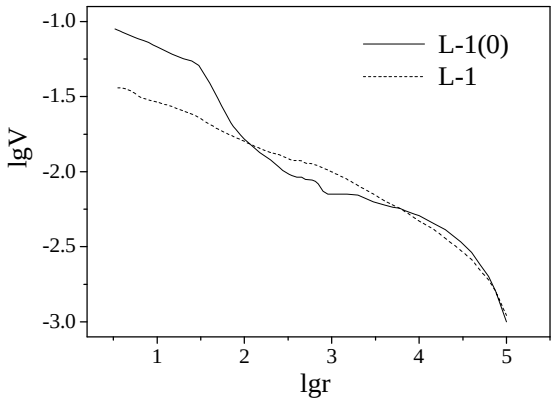

Figure 2. Fractal features of pore structures for L-1 before and after exposure.

The morphology of pores is also an important aspect for the pore structure, which can be used to analyze the complexity of the pore structure within concrete. Fractal dimension has been applied to quantitatively describe the morphology of pores, which can be obtained by the fractal structural model. In this paper, the Space-filling model is used to analyze the fractal features of the pore structure of concrete [15]:

$$\lg V = (3 - D)\lg r + \lg t \tag{1}$$

where V is the cumulative pore volume, r is the pore size, D is the fractal dimension, t is the constant.

According to the experimental results of MIP, $\lg V$ and $\lg r$ are calculated and applied to draw the fractal feature diagram of the pore structure, shown in figure 2 and figure 4. Regression analysis is made for the curves, and the fractal analysis results of the pore structure are shown in table 5. It can be seen that three regression equations have large R^2, which indicates that the curves conform to the equation (1). The fractal dimension D is a parameter to describe the complexity of the pore structure. The higher D represents the more complex internal surface of pores. From the fractal dimension D for L-1(0)~L-3 in Table 5, it is indicated that the OPC concrete before exposure possesses more complex pore internal surface than that after exposure. The OPC concrete after 250 cycles of exposure has more complex pore internal surface than the concrete incorporating fly ash and GBFS.

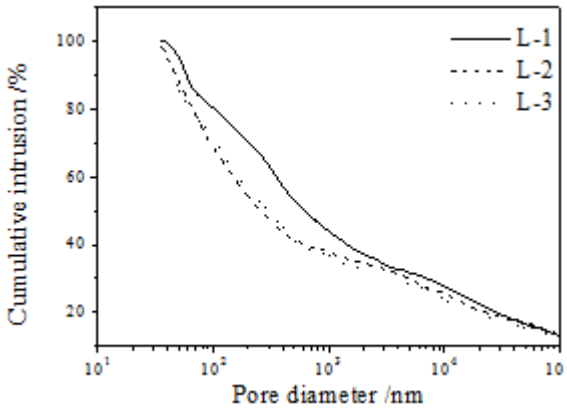

Figure 3. Pore size distribution of concrete after exposure.

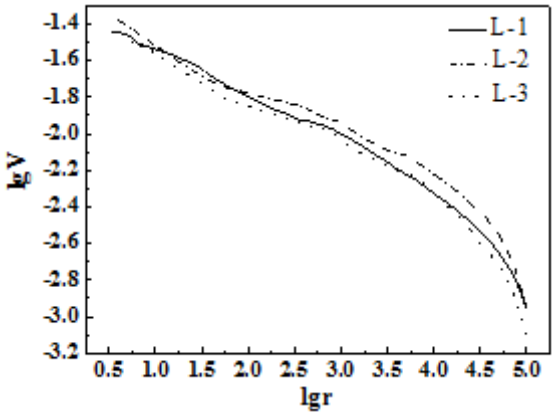

Figure 4. Fractal features of pore structures for concrete after exposure.

Table 5. Fractal analysis of pore structures.

Samples	Regression equation	R^2	D
L-1(0)	y = – 0.3930x – 0.8668	0.9575	3.3930
L-1	y = – 0.2941x – 1.2298	0.9686	3.2941
L-2	y = – 0.2702x – 1.2132	0.9512	3.2702
L-3	y = – 0.2614x – 1.2440	0.9522	3.2614

3.2. X-ray diffraction analysis

To study the corrosive products in the concrete caused by the sulfate attack, the X-ray diffraction analysis was conducted for the powder of paste samples, drawn from three types of mixes. The XRD diffractograms are presented in figures 5-8.

It can be seen that there were relatively low intensity peaks for C-S-H and portlandite in OPC sample subjected to 250 cycles of exposure (figure 6) compared with that obtained before exposure (figure 5). Some amounts of thenardite and gypsum were also detected in figure 6. Peaks for ettringite were intensified after exposure. This signifies that C-S-H and portlandite are consumed, and that gypsum, thenardite and ettringite are produced during cyclic sulfate exposure. There are relatively large intensity peaks for portlandite in OPC sample subjected to 250 cycles of exposure compared with those incorporating mineral admixtures, which is attributed to the pozzolanic reactivity of mineral admixtures. Large quantities of thenardite and gypsum, as well as limited ettringite, were detected in OPC paste. There is largest intensity peak of gypsum in OPC-FA sample, with large amounts of thenardite and little ettringite seen in figure 7; while large quantities of ettringite, thenardite and gypsum are found in the diffractogram of OPC-GBFS sample (figure 8).

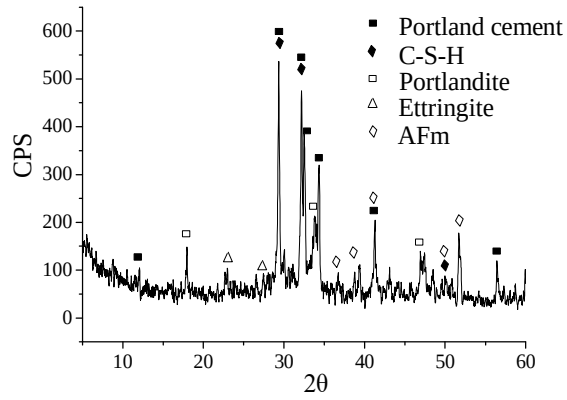

Figure 5. X-ray diffractogram of OPC paste sample before the sulfate exposure.

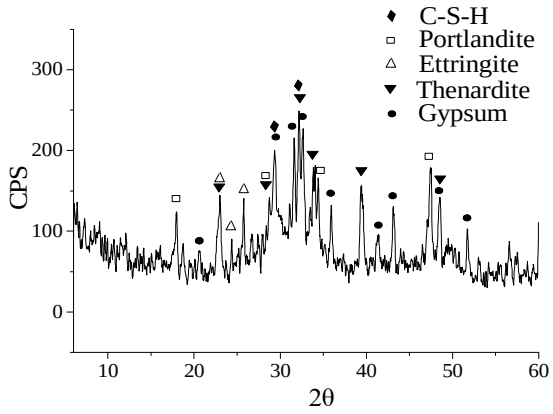

Figure 6. X-ray diffractogram of OPC paste sample subjected to 250 cycles of exposure.

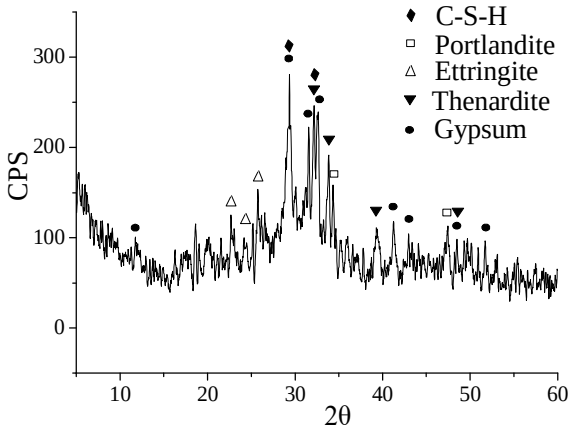

Figure 7. X-ray diffractogram of OPC-FA paste sample subjected to 250 cycles of exposure.

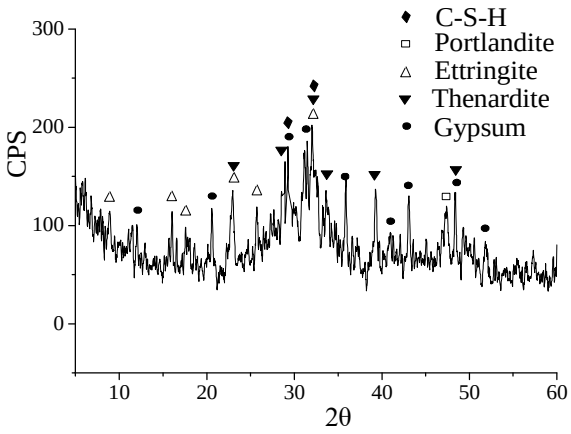

Figure 8. X-ray diffractogram of OPC-GBFS paste sample subjected to 250 cycles of exposure.

3.3. SEM and EDS analysis

To observe the microstructure of the concrete subjected to the sulfate environment, the SEM analysis was applied for the spalling concrete samples after 250 cycles of exposure. In addition, the EDS analysis was conducted to determine the existing compounds after reactions with external corrosive ions.

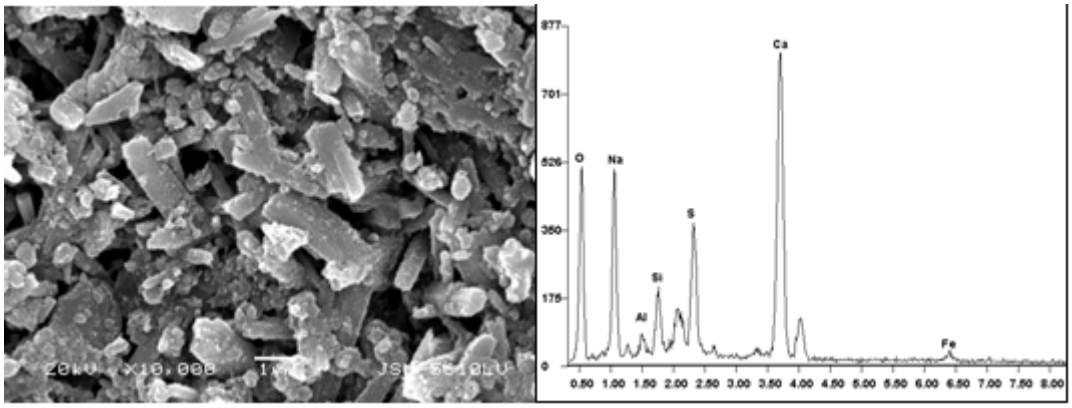

Figure 9. SEM and EDS of OPC concrete sample subjected to 250 cycles of exposure.

The SEM image of OPC concrete sample presents large amounts of white blocky crystals with the fine granular crystals on the surface, as well as small bar-like particles and fine cracks, shown in figure 9. The EDS analysis identifies the existence of sodium, aluminum, silicon, calcium and sulfur.

According to the XRD and EDS results, it is supposed that these white blocky crystals are gypsum and mirabilite, and the fine granular crystals are thenardite, and the bar-like particles are ettringite.

In the SEM image of OPC-FA concrete sample in figure 10, there are abundant white blocky crystals with the fine granular crystals on the surface, as well as the occurrence of fine cracks. The EDS analysis, together with the XRD analysis, confirms that the white blocky crystals are gypsum and mirabilite, and the fine granular crystals are thenardite. Low Al peak in the EDS image signifies the little amount of ettringite.

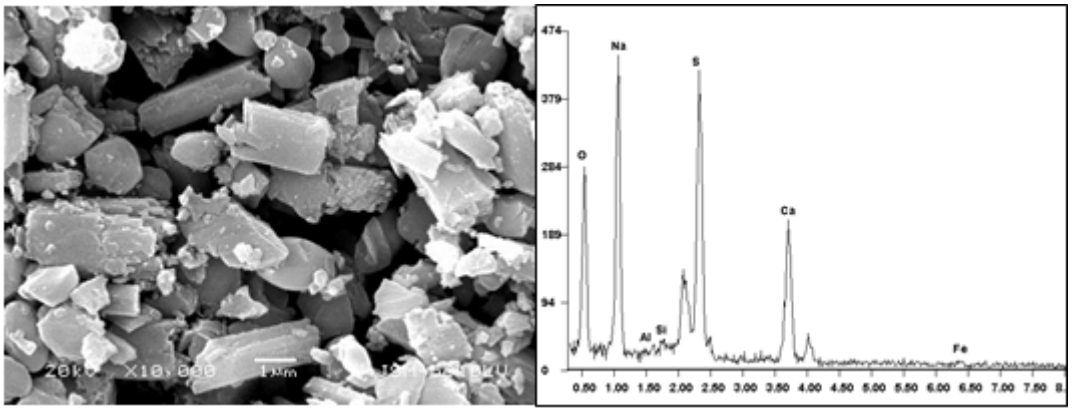

Figure 10. SEM and EDS of OPC-FA concrete sample subjected to 250 cycles of exposure.

Figure 11 shows the SEM and EDS images for the OPC-GBFS sample. There are large quantities of needle-like crystals, as well as some white crystals with the fine granular particles on the surface. According to the EDS and XRD analysis, these needle-like crystals are ettringite, and the white crystals are gypsum and mirabilite, and the fine granular particles are thenardite.

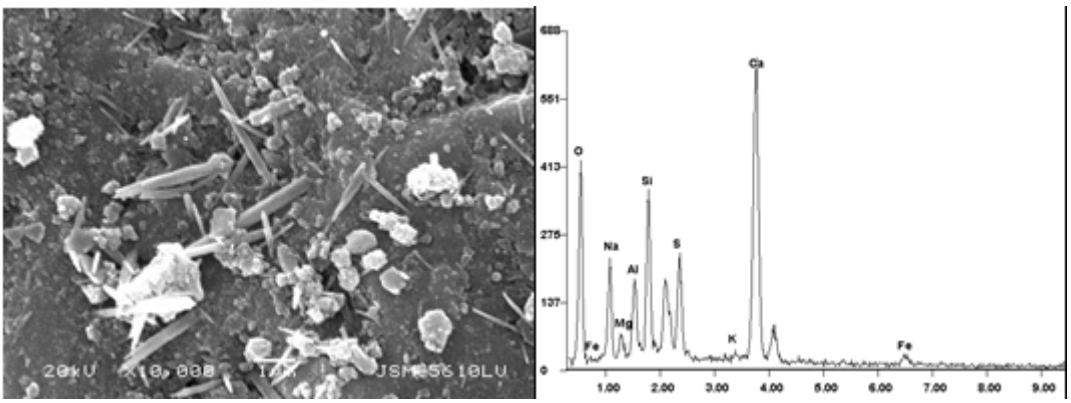

Figure 11. SEM and EDS of OPC-GBFS concrete sample subjected to 250 cycles of exposure.

Therefore, it can be concluded from the XRD, SEM, EDS analysis that sulfates react with the hardened cement paste in the concrete exposed to the sulfate environment. This produces various corrosive products, which is determined by the composition of the cementitious materials. The portlandite in the cement paste is mainly converted to gypsum by reaction with sulfates for OPC concrete and OPC-FA concrete; while for the OPC-GBFS concrete, a large quantity of portlandite reacts with sodium sulfate to form gypsum and ettringite. These expansive products accumulate to cause the occurrence of cracks in the structure, leading to the destruction of concrete.

It is also seen from the SEM images that mirabilite and thenardite are coexisted in various concrete subjected to 250 cycles of exposure. But only abundant thenardite is detected in X-ray diffraction analysis. This may be attributed to the dehydration of mirabilite when making paste samples. It was reported that mirabilite rapidly dehydrated at 20°C (RH<71%) to form thenardite [16]. Thus, it is indicated that repeated hydration and dehydration of sulfates occurred in concrete subjected to the cyclic sulfate exposure may produce additional expansive stress in pores, which aggravates the

demolishment of concrete structure.

4. Conclusions

Incorporation of mineral admixtures improves the sulfate resistance of concrete, which possesses the lower porosity and more micro-pores after 250 cycles of sulfate attack than the OPC concrete. The pore structure of concrete after sulfate exposure possesses the fractal feature, and the OPC concrete after 250 cycles of exposure has more complex pore internal surface than the concrete incorporating fly ash and GBFS.

In the sulfate environment, the portlandite in the cement paste is mainly converted to gypsum by reaction with sulfates for OPC concrete and OPC-FA concrete; while for the OPC-GBFS concrete, a large quantity of portlandite reacts with sodium sulfate to form gypsum and ettringite.

Repeated hydration and dehydration of sulfates occurred in concrete subjected to the cyclic sulfate exposure, may produce additional expansive stress in pores, aggravating the demolishment of concrete structure.

5. References

[1] Mindess S, Young J F, Darwin D et al., 2004 *Concrete 2nd edition*, Chemical Industry Press, Beijing.
[2] Ganjiana E and Pouyab H S *2005 J. Cem. Concr. Res.* **35** 1332-43.
[3] Rafieizonooz M, Salim M R, Mirza J, et al, 2017 *J. Constr. Build. Mater.* **143** 234-46.
[4] Zhang J R, Sun M, Hou D S and Li Z J 2017 *J. Constr. Build. Mater.* **139** 365-73.
[5] Qi B, Gao J M, Chen F and Shen D 2017 *J. Constr. Build. Mater.* **138** 254-62.
[6] Tan Y S, Yu H F, Ma H Y, et al, 2017 *J. Constr. Build. Mater.* **141** 453-60.
[7] Sahmaran M, Erdem T K and Yaman I O 2007 *J. Constr. Build.* Mater. **21** 1771-8.
[8] Shafiq N, Nuruddin M F, Khan S U, Ayub T 2015 *J. Constr. Build.* Mater. **81** 313-23.
[9] Kalla P, Rana A, Chad Y B, et al, 2015 *J. Clean. Prod.* **87** 726-34.
[10] Yu R, Spiesz P and Brouwers H J H 2015 *J. Cem. Concr. Comp.* **55** 383-94.
[11] Yalçınkaya Ç and Yazıcı H 2017 *J. Constr. Build. Mater.* **144** 252-9.
[12] Mermerdaş K and Arbili M M 2015 *J. Constr. Build. Mater.* **94** 371-9.
[13] Yuan X L, Li B X, Cui G, Zhao S C and Zhou M K 2009 *J. Chinese Ceram. Soc.* **37** 1754-9.
[14] Yuan X L, Li B X, Cui G, Zhao S C and Zhou M K 2010 *J. Wuhan Univ. Tech. (Mater. Sci. Ed.).* **25** 1065-9.
[15] Jin S S, Zhang J X and Li S 2009 *J. Concr.* **9** 34-7.
[16] Rodriguez-Navarro C, Doehne E and Sebastian E 2000 *J. Cem. Concr. Res.* **30** 1527-34.

Acknowledgements

Authors gratefully acknowledge the supports from the New Technology Research Projects for 2016 infrastructure engineering of State Grid Corporation of China (No. 40).